American Journal of Polymer Science 2025, 14(3): 46-51
DOI: 10.5923/j.ajps.20251403.02

Nanostructured O-g-C_3N_4/ZnO Composite: Synthesis and Morphological Properties

Gozzal Sidrasulieva[1,*], Altinay Aitmuratova[2], Rayhona Muassarova[2], Nuritdin Kattaev[3], Khamdam Akbarov[3], Sadatdin Tileubaev[4]

[1]DSc Student, Department of Physical Chemistry, National University of Uzbekistan, Tashkent, Uzbekistan
[2]PhD Student, Department of Physical Chemistry, National University of Uzbekistan, Tashkent, Uzbekistan
[3]DSc, Professor, Department of Physical Chemistry, National University of Uzbekistan, Tashkent, Uzbekistan
[4]PhD, Department of Physical Chemistry, Karakalpak State University named after Berdakh

Abstract The O-g-C_3N_4/ZnO photocatalyst was synthesized via a hydrothermal method using zinc oxide derived from local industrial waste and oxygen-doped graphitic carbon nitride (O-g-C3N4). Initially, melamine was calcined at 550 ℃ for four hours to obtain oxygen-doped graphitic carbon nitride. The synthesis process included the conversion of zinc carbonate into zinc nitrate, controlled precipitation using ammonia, hydrothermal treatment at 180 ℃, and subsequent annealing at 350 ℃. SEM analysis revealed the formation of ZnO nanoparticles on the surface of O-g-C_3N_4 nanosheets. The deposition of ZnO nanoparticles on the irregular multilayered carbon nitride sheets caused notable morphological modifications. TEM observations indicated that ZnO nanoparticles distributed on the O-g-C3N4 surface ranged in size from 10 to 50 nm, with distinct nanoscale layering. Elemental mapping and energy-dispersive X-ray spectroscopy (EDS) confirmed the high purity of the composite and the uniform distribution of the main elements (C, N, O, and Zn) throughout the material. Dynamic light scattering (DLS) analysis revealed a bimodal size distribution: the major fraction (44.6%) consisted of particles around 0.1 nm, while the secondary fraction (54.1%) exhibited an average size of ≈ 65 nm.

Keywords O-g-C_3N_4, ZnO, Nanoparticles, Hydrothermal synthesis, Morphology, Photocatalysis

1. Introduction

Photocatalytic technologies are among the most promising approaches for eliminating pollutants, as solar energy represents an inexhaustible, low-cost, and environmentally friendly energy source. Photocatalysis is a catalytic process that occurs on the surface of semiconductor materials under photon irradiation. Despite significant progress in this field, the main research focus remains on enhancing the efficiency and reducing the cost of photocatalysts to enable their large-scale industrial applications.

Various semiconductor materials–such as metal oxides and sulfides (TiO_2, WO_3, CdS, ZnS, ZnO) – have been identified as active photocatalysts for the photodegradation of organic contaminants. Among them, zinc oxide (ZnO) exhibits high performance in the photodegradation of dyes in wastewater. However, ZnO and most oxide-based photocatalysts are mainly active in the ultraviolet region and demonstrate limited overall efficiency.

Current research efforts are directed toward improving the photocatalytic activity of such materials under visible light. Although numerous semiconductors have been developed, most of them show relatively low visible-light activity and suffer from photocorrosion, which restricts their long-term applicability.

To overcome these limitations, a novel metal-free polymeric photocatalyst–graphitic carbon nitride (g-C_3N_4) – was developed, possessing a band gap of approximately 2.7 eV. This material demonstrates outstanding photocatalytic performance in solar-driven hydrogen evolution and in the degradation of organic pollutants under visible light irradiation. Its attractive electronic structure and high thermal and chemical stability make g-C_3N_4 a valuable candidate for photocatalytic applications.

Nevertheless, further enhancement of the photocatalytic efficiency of g-C_3N_4 remains a significant challenge. This can be achieved through structural modification with nanoscale metallic or nonmetallic components that are active under solar illumination, or by forming composites with metal oxides.

The present work aims to synthesise and characterise a nanocomposite based on oxygen-doped graphitic carbon nitride (O-g-C_3N_4) and zinc oxide derived from local industrial waste, a GIAP-10 catalyst used to desulfurise industrial gases.

Particular attention is devoted to the hydrothermal

* Corresponding author:
guzalsidrasulieva@gmail.com (Gozzal Sidrasulieva)
Received: Oct. 2, 2025; Accepted: Oct. 22, 2025; Published: Oct. 31, 2025
Published online at http://journal.sapub.org/ajps

synthesis of the O-g-C_3N_4/ZnO nanostructured composite and its comprehensive characterization by SEM, TEM, EDS, and DLS. The study evaluates particle size, morphology, elemental composition, and aggregation behaviour. Special emphasis is placed on determining particle shape (spherical vs. sheet-like), purity level, and size distribution of ZnO nanoparticles. The obtained results indicate that the synthesized composite combines a stable surface, robust structure, and pronounced heterophase properties, making it a promising photocatalyst for the degradation of organic pollutants in aqueous media.

2. Materials and Methods

2.1. Materials

Melamine and zinc carbonate were used as starting materials. Zinc carbonate was extracted from the industrial waste of the GIAP-10 catalyst (Uzbekistan), which is employed for gas desulfurization processes [18]. Distilled water and ethanol (analytical grade, Sigma-Aldrich) were used for synthesis and washing. Nitric acid (HNO_3, 65%, analytical grade) was employed for dissolving the raw materials, while a 25% aqueous solution of ammonia (NH_4OH) served as the precipitating agent. All reagents were used without additional purification.

2.2. Synthesis of O-g-C_3N_4

To prepare oxygen-doped graphitic carbon nitride, 10 g of melamine was calcined at 550 ℃ for 4 h in air. The resulting material, denoted as O-g-C_3N_4, consisted of nanosheet-like structures enriched with oxygen, forming a light-yellow powder with a layered morphology typical of polymeric carbon nitride.

2.3. Synthesis of Zinc Nitrate

Zinc carbonate obtained from the GIAP-10 waste catalyst was dissolved in nitric acid until the solution reached pH ≈ 7, leading to the formation of a transparent $Zn(NO_3)_2$ solution after complete neutralization of the reaction medium.

2.4. Synthesis of the O-g-C_3N_4/ZnO Nanocomposite

In the first step, the prepared O-g-C_3N_4 photocatalyst was dispersed in 50 mL of distilled water and subjected to ultrasonic treatment at 50 Hz for 6 h to achieve homogeneous dispersion. Then, an appropriate amount of $Zn(NO_3)_2 \cdot 6H_2O$ solution (derived from the GIAP-10 catalyst waste) was added under continuous stirring for 30 min. The resulting mixture was transferred into a 100 mL Teflon-lined autoclave and tightly sealed. Hydrothermal treatment was carried out at 180 ℃ for 12 h. The obtained product was washed three times with distilled water and ethanol, dried at 60 ℃ for 24 h, and subsequently calcined in air at 350 ℃ for 2 h. As a result, a nanostructured O-g-C_3N_4/ZnO composite was obtained, in which ZnO nanoparticles were uniformly anchored onto the surface of O-g-C_3N_4 nanosheets.

2.5. Characterization Techniques

Scanning Electron Microscopy (SEM). The morphology and microstructure of the O-g-C_3N_4/ZnO nanocomposite were examined using a field-emission scanning electron microscope (FE-SEM) at magnifications ranging from ×100 to ×1000. The images were used to analyze particle shape, surface features, and aggregation behavior.

Energy-Dispersive X-ray Spectroscopy (EDS). The constituent elements' elemental composition and spatial distribution were determined using an INCA Energy 300 spectrometer (Oxford Instruments, UK) coupled with the SEM system.

Transmission Electron Microscopy (TEM). High-resolution TEM analysis was conducted to study the size distribution and morphology of ZnO nanoparticles within the composite. Images were captured at scales between 100–200 nm, allowing the identification of both spherical and sheet-like morphologies.

Dynamic Light Scattering (DLS). Dynamic light scattering measurements were performed to determine the hydrodynamic size distribution of particles in a colloidal suspension. The DLS method allows the sensitive determination of particle sizes in the range of approximately 1–1000 nm, covering both nanodispersed and submicron systems. The technique is based on analysing fluctuations in scattered light intensity caused by the Brownian motion of particles. The obtained data were used to evaluate hydrodynamic size distributions and construct bimodal profiles reflecting the presence of both primary nanoparticles and secondary aggregates [19].

3. Results and Discussion

The morphological and dimensional characteristics of the synthesized nanocomposite were comprehensively investigated using a combination of complementary techniques, including scanning electron microscopy (SEM), transmission electron microscopy (TEM), energy-dispersive X-ray spectroscopy (EDS), and dynamic light scattering (DLS). This integrated approach enabled a detailed analysis of particle morphology, surface structure, aggregation behavior, elemental composition, and particle size distribution. The results demonstrated that the hydrothermal synthesis based on oxygen-doped carbon nitride and zinc oxide derived from local industrial waste led to a nanocomposite with pronounced structural heterogeneity. ZnO nanoparticles were uniformly distributed across the lamellar O-g-C_3N_4 surface, significantly influencing the physicochemical properties of the material.

3.1. Surface Morphology (SEM Analysis)

SEM images revealed that the synthesized oxygen-doped graphitic carbon nitride (O-g-C_3N_4) exhibited a typical multilayered, sheet-like morphology. The surface was porous and composed of intertwined fibrous sheets with pronounced wrinkles and irregularities, contributing to an increased specific surface area. The thickness of individual sheets ranged from 40 to 80 nm, while their lateral dimensions were 500–800 nm.

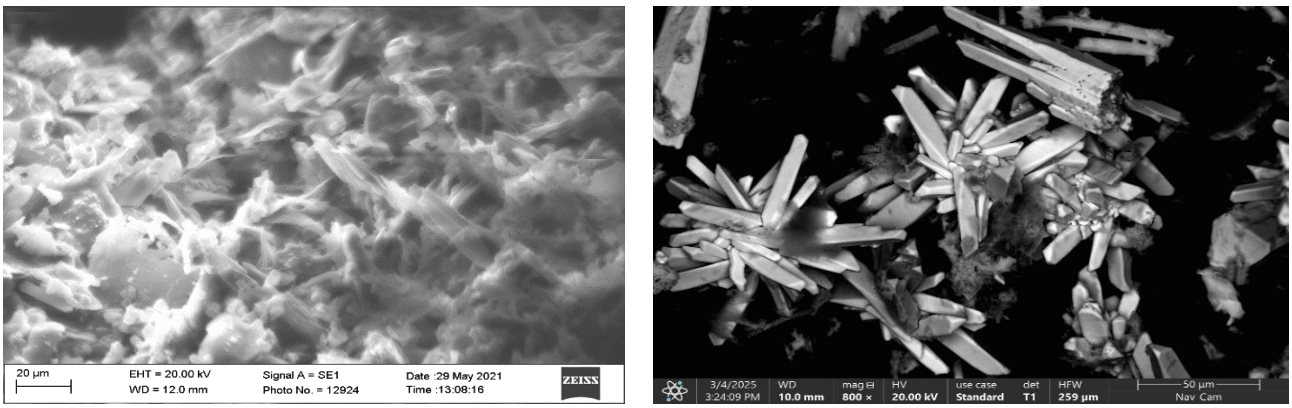

Figure 1. Morphology: (a) O-g-C_3N_4; (b) O-g-C_3N_4/ZnO composite

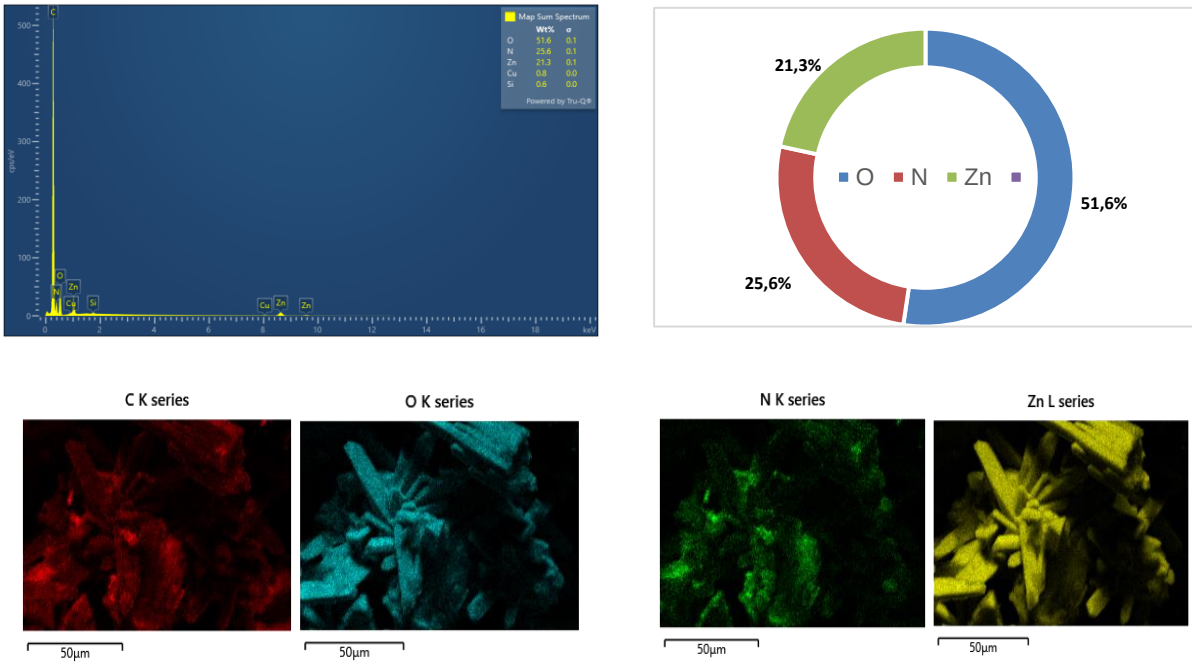

Figure 2. EDS spectrum and elemental mapping of the O-g-C_3N_4/ZnO composite

This microstructure indicates a high degree of dispersion and favourable conditions for charge carrier transport. Owing to the high surface area and porous nature, O-g-C_3N_4 is expected to exhibit enhanced photocatalytic activity. Upon incorporation of ZnO nanoparticles, the morphology of O-g-C_3N_4 changed significantly. The composite surface displayed spherical and partially aggregated ZnO nanoparticles with sizes ranging from 10 to 50 nm, uniformly distributed across the wrinkled nanosheets (Fig. 1). Despite these structural changes, the original layered framework of O-g-C_3N_4 was preserved, suggesting that the carbon nitride matrix acts as an effective substrate for ZnO deposition.

3.2. Elemental Composition (EDS Analysis)

Energy-dispersive X-ray spectroscopy (EDS) confirmed the presence of four primary elements – C, N, O, and Zn – in the O-g-C_3N_4/ZnO composite (Fig. 2). Quantitative analysis revealed that the material contains 31.6 wt% O, 25.6 wt% N, 21.6 wt% Zn, and 20.6 wt% C, with trace amounts of Cu (0.6 wt%) and S (0.1 wt%) attributed to the substrate and probe artifacts. The resulting atomic ratio Zn:O ≈ 1:1.05 closely matches the stoichiometry of ZnO, confirming the formation of a chemically balanced oxide phase.

Elemental mapping demonstrated a uniform spatial distribution of all major elements throughout the hybrid matrix, without visible segregation zones or impurity phases [20]. The relatively high contents of nitrogen and carbon correspond to the graphitic carbon nitride framework, while oxygen and zinc peaks represent the ZnO nanoparticles uniformly deposited over O-g-C_3N_4 nanosheets. The oxygen enrichment of the composite, compared to pristine g-C_3N_4, indicates successful oxygen doping during calcination, which may contribute to improved charge separation and enhanced photocatalytic activity.

The EDS spectrum exhibited distinct peaks at 0.28 keV (C Kα), 0.39 keV (N Kα), 0.52 keV (O Kα), and 1.01 keV / 8.64

keV (Zn Lα / Kα). The absence of extraneous peaks confirmed the high chemical purity of the synthesized composite. Such compositional homogeneity and purity are essential for achieving stable heterojunctions between ZnO and O-g-C_3N_4, facilitating efficient charge transfer and increasing photocatalytic efficiency.

3.3. Structural Analysis (TEM Observations)

High-resolution transmission electron microscopy (HRTEM) provided detailed insight into the internal architecture and crystallinity of the synthesized O-g-C_3N_4/ZnO nanocomposite (Fig. 3). At magnifications of 94 000× to 120 000×, individual ZnO nanoparticles were clearly observed to be uniformly anchored on the layered surface of O-g-C_3N_4. The measured particle diameters ranged from 11.6 nm to 57.5 nm, with most crystallites falling within 15–35 nm, confirming a narrow nanoscale size distribution consistent with controlled nucleation during hydrothermal synthesis.

The nanoparticles exhibited distinct lattice fringes with interplanar spacings of 0.247 nm and 0.281 nm, which correspond to the (101) and (100) planes of wurtzite ZnO, respectively. The presence of well-resolved fringes and the absence of amorphous halos indicate a high degree of crystallinity. The O-g-C_3N_4 matrix appears as thin, semi-transparent nanosheets with a corrugated morphology that serves as an effective substrate for ZnO growth.

Clusters up to 250–300 nm were occasionally observed, resulting from localized aggregation of ZnO nanoparticles, yet the overall dispersion remained homogeneous. The intimate interfacial contact between ZnO and O-g-C_3N_4 facilitates efficient charge migration across the heterojunction interface, reducing recombination of photoinduced electron–hole pairs.

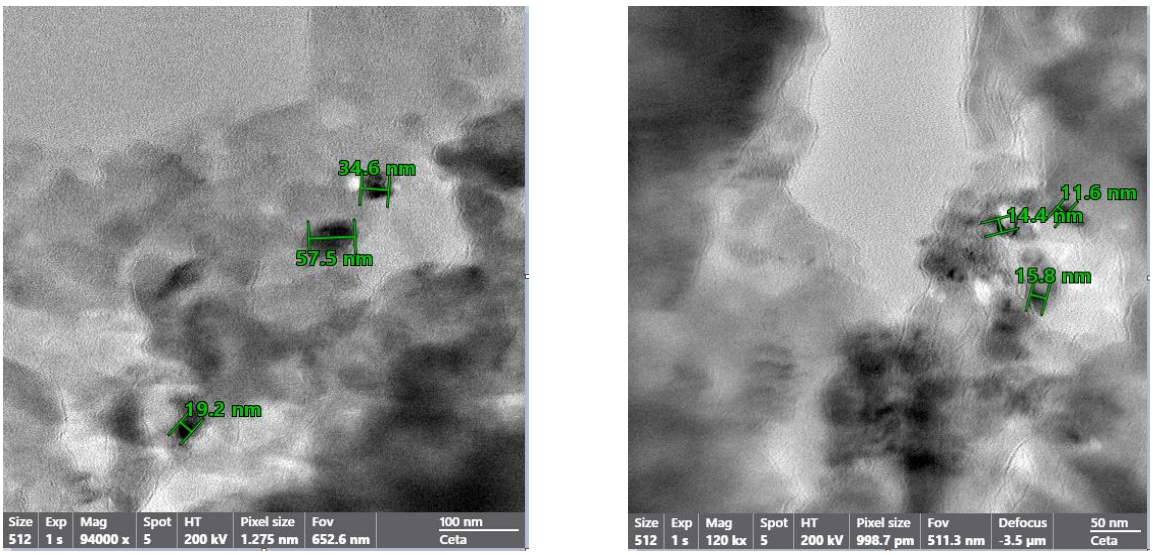

Figure 3. TEM images of the O-g-C_3N_4/ZnO composite

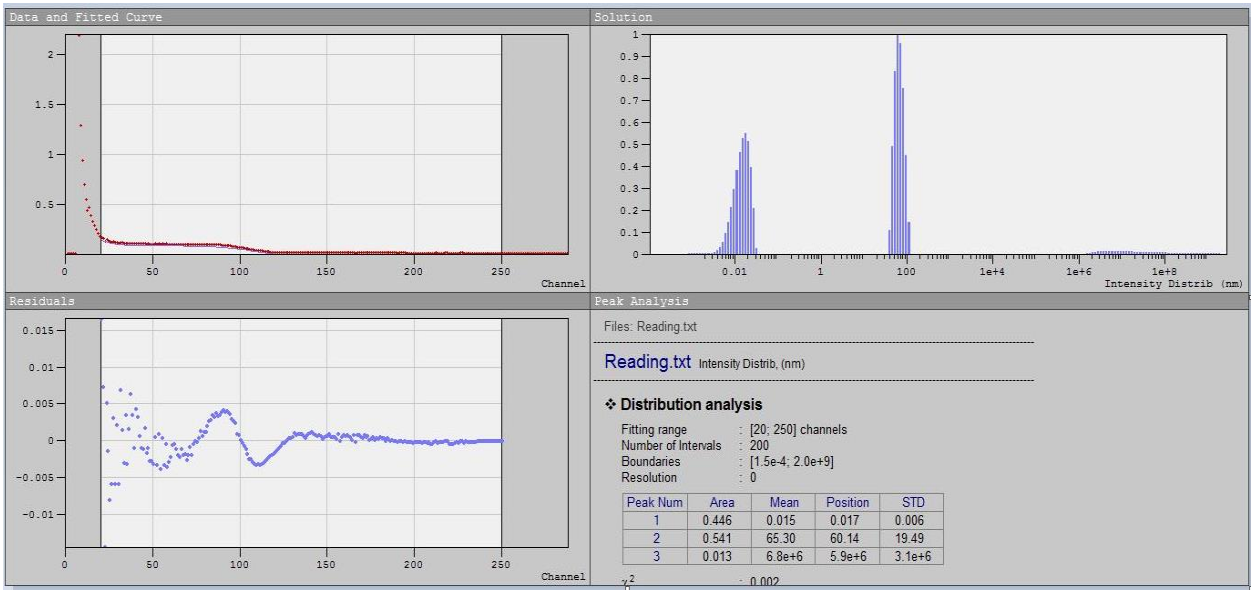

Figure 4. Particle size distribution of O-g-C_3N_4/ZnO nanoparticles obtained by DLS

These structural characteristics are in excellent agreement with XRD data, confirming the coexistence of crystalline ZnO (wurtzite structure) and partially ordered O-g-C_3N_4 layers. The combined TEM and HRTEM analyses highlight that the composite exhibits uniform ZnO nanoparticle distribution, high crystallinity, and strong interfacial coupling, all of which are essential for enhanced photocatalytic performance under visible-light irradiation.

3.4. Particle Size Distribution (DLS Analysis)

Dynamic light scattering (DLS) was employed to determine the hydrodynamic size distribution of particles in suspension. According to the analysis, the composite contained particles belonging to two main size populations, forming a bimodal distribution pattern: the primary fraction (~44.6%) consisted of nanoparticles with an average size of approximately 0.1 nm, and the secondary fraction (~54.1%) corresponded to larger particles with an average diameter of 65 nm. Upon dilution of the suspension, an increase in polydispersity and mean particle size was observed, attributed to agglomeration of nanoparticles in the aqueous–alcohol medium.

The hydrodynamic radii obtained from DLS were slightly larger than those measured by TEM, which can be explained by the formation of solvation shells around nanoparticles due to polarization of the surrounding solvent molecules. These solvation effects stabilize the colloidal system and prevent rapid aggregation.

The combined results of SEM, TEM, EDS, and DLS analyses confirm that the synthesized O-g-C_3N_4/ZnO composite is a nanostructured material primarily composed of particles 10–50 nm in size, prone to forming secondary aggregates and clusters. The coexistence of spherical and sheet-like morphologies leads to a highly porous structure with an expanded specific surface area. Such structural diversity and chemical purity make the composite a promising candidate for various applications, particularly photocatalysis and chemical sensing. The developed nanostructure facilitates efficient light absorption and accelerates surface reactions, thereby enhancing organic pollutants' degradation rate. Overall, the morphological analysis validates the effectiveness of the proposed hydrothermal synthesis route for producing oxygen-doped graphitic carbon nitride decorated with ZnO nanoparticles derived from local industrial waste.

4. Conclusions

A nanostructured O-g-C_3N_4/ZnO composite was successfully synthesized via a sustainable hydrothermal route using zinc oxide derived from local industrial waste and oxygen-doped graphitic carbon nitride as precursors. The multi-step process – including zinc carbonate conversion, ammonia-assisted precipitation, hydrothermal treatment at 180 ℃, and annealing at 350 ℃ – yielded a high-purity hybrid photocatalyst with excellent structural stability.

Structural and compositional analyses confirmed that the composite consists of ZnO nanoparticles (11.6–57.5 nm) uniformly distributed over O-g-C_3N_4 nanosheets. HRTEM revealed distinct lattice fringes corresponding to the (101) and (100) planes of wurtzite ZnO, while EDS analysis verified homogeneous elemental distribution (C = 20.6 wt%, N = 25.6 wt%, O = 31.6 wt%, Zn = 21.6 wt%) and stoichiometric Zn:O ≈ 1:1. DLS results indicated a bimodal particle size distribution, reflecting the coexistence of primary nanoparticles and secondary aggregates.

The intimate interfacial contact between ZnO and O-g-C_3N_4 promotes efficient charge transfer and suppresses electron–hole recombination, which is expected to enhance photocatalytic performance under visible light. The use of GIAP-10 catalyst waste as a zinc precursor demonstrates an environmentally responsible and cost-effective synthesis strategy aligned with green chemistry and sustainable materials development.

REFERENCES

[1] Fujishima, A., & Honda, K. (1972). Electrochemical photolysis of water at a semiconductor electrode. Nature, 238, 37–38.

[2] Kamat, P. V. (1993). Photochemistry on nonreactive and reactive (semiconductor) surfaces. Chemical Reviews, 93, 267–300.

[3] Hagfeldt, A., & Grätzel, M. (1995). Light-induced redox reactions in nanocrystalline systems. Chemical Reviews, 95, 49–68.

[4] Hoffmann, M. R., Martin, S. T., Choi, W. Y., & Bahnemann, D. W. (1995). Environmental applications of semiconductor photocatalysis. Chemical Reviews, 95, 69–96.

[5] Linsebigler, A. L., Lu, G. Q., & Yates, J. T. Jr. (1995). Photocatalysis on TiO_2 surfaces: Principles, mechanisms, and selected results. Chemical Reviews, 95, 735–758.

[6] Steven, N. F., & Bard, A. J. (1977). Semiconductor electrodes and photoelectrochemistry. Journal of the American Chemical Society, 99, 303–310.

[7] Thompson, T. L., & Yates, J. T. Jr. (2006). Surface science studies of the photoactivation of TiO_2 – New photochemical processes. Chemical Reviews, 106, 4428–4453.

[8] Mills, A., & Hunte, S. L. (1997). An overview of semiconductor photocatalysis. Journal of Photochemistry and Photobiology A: Chemistry, 108, 1–35.

[9] Ayoub, K., van Hullebusch, E. D., Cassir, M., & Bermond, A. (2010). Application of advanced oxidation processes for wastewater treatment. Journal of Hazardous Materials, 178, 10–17.

[10] Akpan, U. G., & Hameed, B. H. (2009). Parameters affecting the photocatalytic degradation of dyes using TiO_2-based photocatalysts: A review. Journal of Hazardous Materials, 170, 520–529.

[11] Li, Y., Sasaki, T., Shimizu, Y., & Koshizaki, N. (2008). Fabrication of ZnO nanostructures by laser ablation in liquids and their photocatalytic properties. Journal of the American Chemical Society, 130, 14755–14762.

[12] Li, Y., Sasaki, T., Shimizu, Y., & Koshizaki, N. (2008). ZnO nanostructures with different morphologies obtained by laser ablation in liquids: Comparison of photocatalytic activity. Small, 4, 2286–2290.

[13] Yeber, M. C., Rodr guez, J., Freer, J., Dur n, N., & Mansilla, H. D. (2000). Photocatalytic degradation of dyes over TiO_2 and ZnO suspensions. Chemosphere, 41, 1193–1199.

[14] Khodja, A. A., Sehili, T., Pilichowski, J. F., & Boule, P. (2001). Photocatalytic degradation of 2-phenylphenol on TiO_2 and ZnO suspensions. Journal of Photochemistry and Photobiology A: Chemistry, 141, 231–239.

[15] Ye, C., Bando, Y., Shen, G., & Golberg, D. (2006). Thickness -controlled growth and properties of ZnO nanobelts. Journal of Physical Chemistry B, 110, 15146–15151.

[16] Cao, B., & Cai, W. (2007). Enhanced photocatalytic activity of ZnO nanorod arrays fabricated by chemical vapor deposition. Journal of Physical Chemistry C, 112, 680–685.

[17] Wang, X. C., Maeda, K., Thomas, A., Takanabe, K., Xin, G., Carlsson, J. M., Domen, K., & Antonietti, M. (2009). A metal-free polymeric photocatalyst for hydrogen production from water under visible light. Nature Materials, 8, 76–80.

[18] Cullity, B. D., & Stock, S. R. (2001). Elements of X-Ray Diffraction (3rd ed., pp. 50–52). Prentice Hall.

[19] Tang, E., et al. (2011). Influence of surface modification on the dispersion stability of TiO_2 nanoparticles in aqueous suspension. Journal of Nanoparticle Research, 13, 3169–3178.

[20] Kumar, S., et al. (2014). Synthesis and characterization of ZnO–graphitic carbon nitride nanocomposites for enhanced photocatalytic activity. Journal of Hazardous Materials, 275, 200–210.

[21] Zhang, J.-H., Hou, Y.-J., Wang, S.-J., Zhu, X., Zhu, Ch.-Y., Wang, Zh., Li, Ch.-J., Jiang, J.-J., Wang, H.-P., Pan, M., & Sua, C.-Y. (2018). A facile method for scalable synthesis of ultrathin g-C_3N_4 nanosheets for efficient hydrogen production. Journal of Materials Chemistry A, 6(37), 18020–18029.